Environment International 208 (2026) 110112

Contents lists available at ScienceDirect

Environment International

journal homepage: www.elsevier.com/locate/envint

Full length article

Metabolic effects and biotransformation of perfluorohexyloctane in human hepatocytes

Andi Alijagic [a,b,c], Jade Chaker [a], João Marcos G. Barbosa [a], Daniel Duberg [a], Victor Castro-Alves [a], Alex M. Dickens [d,e], Matej Orešič [c,d,f], Tuulia Hyötyläinen [a,*]

[a] Man-Technology-Environment (MTM) Research Centre, School of Science and Technology, Örebro University, SE-701 82 Örebro, Sweden
[b] Inflammatory Response and Infection Susceptibility Centre (iRiSC), Örebro University, Örebro SE-701 82, Sweden
[c] School of Medical Sciences, Faculty of Medicine and Health, Örebro University, SE-701 82 Örebro, Sweden
[d] Turku Centre for Biotechnology, University of Turku and Åbo Akademi University, FI-20520 Turku, Finland
[e] Department of Chemistry, University of Turku FI-20500 Turku, Finland
[f] Department of Life Technologies, University of Turku FI-20014 Turku, Finland

ARTICLE INFO

Keywords:
HepaRG
Lipidomics
Liver metabolism
Metabolomics
Perfluorohexyloctane
PFAS

ABSTRACT

Perfluorohexyloctane (F6H8) is a semifluorinated alkane recently approved for ophthalmic treatment of dry eye disease. Although considered locally safe for topical use, its structural similarity to persistent per- and polyfluoroalkyl substances (PFAS) raises concerns about systemic accumulation and long-term toxicity. To investigate potential hepatic effects, we examined the metabolic impact of F6H8 exposure in human HepaRG hepatocytes across a broad concentration range representing short- and long-term exposure scenarios. Combined targeted and untargeted metabolic profiling by ultra-high-performance liquid chromatography–quadrupole time-of-flight mass spectrometry (UHPLC-QTOFMS) was performed on intracellular extracts and extracellular media. F6H8 induced pronounced, concentration-dependent metabolic alterations, many of which exhibited non-monotonic responses. Low concentrations primarily affected amino acid, fatty acid, and lipid metabolism, while central carbon metabolism was disrupted only at the highest exposures. Notably, a putative biotransformation product, perfluorohexyloctanoic acid, was detected, suggesting metabolic persistence and conversion to a PFAS-like structure. This metabolite showed strong associations with cellular metabolic profiles and elicited metabolic changes that only partially overlapped with those induced by the parent compound, indicating distinct biological activity following biotransformation. These findings indicate that F6H8 elicits broad metabolic reprogramming and may not be metabolically inert as previously assumed. Given its clinical use and structural similarity to persistent fluorochemicals, the results highlight the need for comprehensive, long-term safety assessment of F6H8 and related semifluorinated alkanes.

1. Introduction

Perfluorohexyloctane (F6H8) is a semifluorinated alkane approved for ophthalmic use and increasingly incorporated into ophthalmic formulations for the treatment of dry eye disease, particularly those associated with meibomian gland dysfunction. Clinical studies have demonstrated its efficacy and short-term safety following topical administration (Steven et al., 2015; Tauber J.; Berdy G. J.; Wirta D. L.; Krosser S.; Vittitow J. L.; Group G. S, 2023); however, its broader toxicological profile remains poorly characterized. Owing to its classification within the per- and polyfluoroalkyl substance (PFAS) class, F6H8 shares physicochemical features with other highly fluorinated compounds that are known to persist in biological systems and the environment, raising concerns regarding potential systemic accumulation and long-term health effects.

Compared to well-studied PFAS such as perfluorooctanoic acid (PFOA) and perfluorooctane sulfonate (PFOS), the metabolic fate, biotransformation potential, and potential cellular effects of F6H8 remain poorly understood. Existing toxicological data are limited to short-term clinical safety evaluations under ophthalmic exposure scenarios. Notably, structurally related semifluorinated alkanes with longer hydrocarbon tails have been used in industrial applications such as ski

* Corresponding author at: School of Science and Technology, Örebro University, 70182 Örebro, Sweden.
E-mail address: tuulia.hyotylainen@oru.se (T. Hyötyläinen).

https://doi.org/10.1016/j.envint.2026.110112
Received 31 October 2025; Received in revised form 15 January 2026; Accepted 26 January 2026
Available online 29 January 2026

waxes—a practice now restricted or banned in many countries because of concerns over environmental persistence and bioaccumulation. Analyses of ski wax formulations have shown that semifluorinated alkanes commonly contain fluorinated chains of F6H16, F10H16, F12H16, F14H16 and F16H16 (Plassmann and Berger, 2010).

There is limited data on biological effects of F6H8 from *vivo* studies. Reported nonclinical pharmacology and toxicology studies include two studies in rabbits and two in rats (Rhea Lloyd and Chambers, 2023). The endpoints analyzed were toxicity in two of the studies and embryofetal developmental (EFD) toxicity in the other two. In a 26-week ocular toxicity study in rabbits, ocular instillation of F6H8 ophthalmic solution (427.8 mg/day, four times daily bilaterally for up to 26 weeks) was well tolerated and did not induce any ocular or systemic signs of toxicity. In another 28-day oral toxicity study in rats, daily oral administration of at doses up to 2000 mg/kg/ for 28 days were well tolerated and did not produce F6H8 related toxicity. In an EFD toxicity study in rats, daily oral administration of F6H8 at doses up to 2000 mg/kg/day to pregnant Wistar rats during the period of organogenesis was well tolerated with no toxicological effects on maternal or embryofetal parameters (Rhea Lloyd and Chambers, 2023). However, in an EFD toxicity study in rabbits, following daily oral administration of F6H8 (0, 250, 500 and 1000 mg/kg/day) to pregnant female New Zealand white (NZW) rabbits during the period of organogenesis, there were abortions in all treated groups, compared with no abortion in the control group (Rhea Lloyd and Chambers, 2023). In animals treated with F6H8, normal weight gain from birth to adulthood was reduced in a dose-dependent manner. Reduced food consumption was also noted at a dose-related trend. There were higher incidences of reduced fecal output, soft feces and/or absent urine in all groups during the dosing period compared with the control group. Consistent with maternal toxicity, mean fetal weight was reduced in all treated groups compared with the concurrent control group. There was no increase in embryofetal death nor test article-related delay in skeletal ossification in any treated group, however, there were more fetal malformations (external, visceral, and/or skeletal) in the low, mid and high dose treatment groups as compared with the control group. In a rat study using F6H8-based propofol, elevation of liver enzyme alanine-aminotransferase (ALT) after exposure to F6H8-based propofol was observed in absence of histological changes in the liver, in comparison with conventional propofol emulsion (Tsagogiorgas et al., 2015). Viability and proliferation of cultured human corneal endothelial cells and human retinal pigment epithelial cells were decreased after incubation with F6H8, which was likely due to high lipophilicity of F6H8 interactions with cellular lipoprotein membranes (Mertens et al., 2002). In a recent zebrafish model study, F6H8 was shown to induce a hypoactive embryonic photomotor response, suggesting potential developmental neurotoxicity (Truong et al., 2022). Clinical studies in humans have been primarily focused on ocular endpoints and symptom relief, lacking investigation of systemic and long-term chronic exposure effects.

There is very limited data on adsorption, organ distribution, and excretion of F6H8. In a rabbit study, labelled F6H8 was administered into eyes of the rabbits, and the concentration of F6H8 was investigated in ocular tissues, blood and plasma using radioactivity by liquid Scintillation counting (Kroesser et al., 2018; Krösser et al., 2025). Following a single dose, plasma concentrations increased to 973 ng/g at 4 h and declined to 360 ng/g by 24 h, suggesting potential accumulation with chronic dosing of multiple times daily. Compounds with similar structure to F6H8, namely $C_6F_{13}C=CHC_{10}H_{21}$ (F6H10E), has been investigated with regards to the organ distribution and organ retention time in rats (Zarif et al., 1994). The F6H10E content in the liver peaked one day after administration (seven days for the spleen). At a dose of 3.6 g/kg body weight, the hepatic half-life of F6H10E was estimated at 25 ± 5 days (Zarif et al., 1994). In addition, saturated alkanes, *i.e.*, compounds with structure otherwise identical, but with no fluorine atoms, has been shown to enrich in the liver, where they are metabolized into carboxylic acids with the same chain length (Cravedi and Tulliez, 1986; McCarthy, 1964; Tulliez and Bories, 1978). The liver concentrations were ca. two times higher than in the blood. According to the FDA's *Report on the Use of PFAS in Cosmetic Products and Associated Risks* (2026), perfluorohexane, which shares structural similarities with F6H8, was observed to undergo metabolic transformation in vitro*/in vivo*, suggesting limited but measurable biotransformation under certain conditions.

Taken together, toxicological and chronic exposure data on F6H8 remain scarce, particularly regarding its biological effects. Existing investigations have primarily focused on acute toxicity, which may be insufficient to reveal the consequences of long-term chronic exposures, as adverse health effects can take extended periods to develop. To date, no published studies have addressed the metabolic effects of F6H8. The US Food and Drug Administration (FDA) approval documents state that F6H8 is not metabolized by human lisuver microsomes, however, no supporting data or peer-reviewed studies have been published.

Related work has demonstrated that semifluorinated alkanes can interact with phospholipids and integrate into lipid bilayers (Sabín et al., 2006). When co-dispersed with phospholipids, the lipophobic fluorinated compounds have been shown to aggregate and form a phase-separated fluorinated core within the membrane (Ferro and Krafft, 2002). Thus, even if F6H8 itself were metabolically inert, it could still alter cellular metabolism by modifying membrane structure and function.

To address this critical knowledge gap, we investigated the metabolic effects of F6H8 exposure in human hepatocytes, given the the liver is a primary site of uptake, accumulation, and metabolism for lipophilic xenobiotics, and as structurally related alkanes and semifluorinated compounds have been shown to enrich in hepatic tissue. This makes hepatocyte models particularly relevant for probing metabolic perturbations and potential biotransformation of F6H8. Using comprehensive mass spectrometry (MS) based, combined targeted and untargeted metabolic profiling, we examined how F6H8 influences cellular metabolism across a wide concentration range and assessed possible biotransformation of the compound. Both intracellular extracts and extracellular media were analyzed to provide an integrated view of exposure-related metabolic changes. Our findings offer foundational toxicological insight into this widely used but poorly understood compound and inform future risk assessment of F6H8 and related fluorinated substances.

2. Materials and methods

2.1. Chemicals

All solvents were HPLC grade or LC-MS grade, from Honeywell (Morris Plains, NJ, USA), Fisher Scientific (Waltham, MA, USA) or Sigma-Aldrich (St. Louis, MO, USA). MS grade ammonium acetate and reagent grade formic acid were also from Sigma-Aldrich (St. Louis, MO, USA). The lipid standards were from Avanti Polar Lipids Inc. (Alabaster, AL, USA). ^{13}C-labeled PFAS internal standards (IS), ^{13}C-labeled performance standards, and native calibration standards (perfluorocarboxylic acids [PFCAs] and perflurosulfonic acids [PFSAs]) were purchased from Wellington Laboratories (Guelph, Ontario, Canada). One native performance standard, 7H-dodecafluoroheptanoic acid, was purchased from ABCR (Karlsruhe, Germany). Cholic acid (CA), chenodeoxycholic acid (CDCA), deoxycholic acid (DCA), dehydrocholic Acid (DHCA), glycocjolic acid (GCA), glyco chenodeoxycholic acid (GCDCA), lithocholic acid (LCA), taurocholic acid (TCA), taurochenodeoxycholic acid (TCDCA), taurodeoxycholic acid TDCA, taurodehydrocholic acid (TDHCA), taurohyocholic acid (THCA), taurohyodeoxycholic acid (THDCA), taurolithocholic acid (TLCA), and tauroursocholic acid (TUDCA) were obtained from Sigma-Aldrich (St. Luis, MO, USA), hyodeoxycholic acid (HDCA), hyocholic acid (HCA), murocholic acids α, β and ω (αMCA, βMCA, ωMCA), 7-oxohyodeoxycholic acid (7-oxo-HDCA), 7-oxodeoxycholic acid (7-oxo-DCA), 12-oxo lithocholic acid (12-oxo-

Table1
LC-MS conditions for the two methods used in the study.

Conditions	Polar/semipolar compounds: Method 1	Lipidomics: Method 2
Injection volume	2 μl	1 μl
Column	C18 precolumn (Waters Corporation, Wexford, Ireland) and an inline filter, pore size 0,2 μm (Waters Corporation, Wexford, Ireland) + ACQUITY UPLC® BEH C18 column (2.1 mm × 100 mm, particle size 1.7 μm) by Waters (Milford, MA, USA)	C18 precolumn (Waters Corporation, Wexford, Ireland) and an inline filter, pore size 0,2 μm (Waters Corporation, Wexford, Ireland) + ACQUITY UPLC® BEH C18 column (2.1 mm × 100 mm, particle size 1.7 μm) by Waters (Milford, MA, USA)
Mobile phases	A H_2O:MeOH (v/v 70:30) with 2 mM ammonium acetate B MeOH with containing 2 mM ammonium acetate	A 10 mM ammonium acetate and 0.1 % Formic Acid in H_2O B Acetonitrile:Isopropanol (v/v 1:1) with 0.1 % Formic Acid and 10 mM ammonium acetate
Gradient	• 0–1.5 min: B was increased from 5 % to 30 % • 1.5–4.5 min: B increased to 70 % • 4.5–7.5 min: B increased to 100 % and held for 5.5 min. • A post-time of 6 min	• 0–2 min: B was increased from 35 % to 80 % • 2–7 min: B increased to 100 % • 7–14 min: B was held at 100 % • A post-time of 7 min
Flow rate	0.4 $mLmin^{-1}$	0.4 $mLmin^{-1}$
MS conditions	ESI ionization source with capillary voltage 1.5 kV and cone voltage 40 V. N2 as desolvation gas and cone gas. Desolvation gas temperature and flow was set to 550 °C and 1000 Lh^{-1}, respectively. Source temperature was set to 150 °C and cone gas flow was set to 50 Lh^{-1}. *m/z* range 50–1200 in negative ion mode.	Dual ESI ionization source with capillary voltage 3.64 kV, nozzle voltage 1500 V, N2 pressure in the nebulized was 21 psi and the N2 flow rate and temperature as sheath gas was 11 Lmin-1 and 379 °C, respectively. Drying gas flow was set to 10 $Lmin^{-1}$ and temperature to 193 °C. *m/z* range 100–1700 in positive ion mode.

LCA), tauromurocholic acid), murocholic acids α, β and ω (TαMCA, TβMCA, TωMCA), glycodehydrocholic acid (GDHCA), glycohyocholic acid (GHCA), and glycohyodeoxycholic acid) GHDCA from Steraloids (Newport, RI, U.S.A), glycolithocholic acid (GLCA) and glycoursocholic acid (GUDCA) from Calbiochem (Gibbstown, NJ, U.S.A), and glycodeoxycholic acid (GDCA) and ursocholic acid (UDCA) from Fluka (Buchs, Switzerland). Internal standards CA-d4, LCA-d4, UDCA-d4, CDCA-d4, DCA-d4, GCA-d4, GLCA-d4, GUDCA-d4 and GCDCA-d4 were obtained from Qmx laboratories Ltd. (Essex, UK). For quality assurance (QA), standard reference material serum NIST SRM 1950 (for lipidomics and metabolomics) and 1957 (for PFAS and bile acids) was purchased from the National Institute of Standards and Technology (NIST) at the US Department of Commerce (Washington, DC, USA).

Perfluorohexyloctane was purchased from a local pharmacy. It was analyzed by nuclear magnetic resonance (NMR) to verify its purity. The main compound had both fluorine and protein peaks that aligned with previous literature values (Stolowich et al., 2023). However, there was smaller fluorine peaks observed (**Supplementary Fig. 1**) suggesting that there is other fluorinated species contained in the eye drop solution. The NMR was run on a Bruker Advance III 500 system equipped with a smart probe. Both F19 and 1H NMR was performed to confirm the structure of the eyedrop solution.

2.2. Cell culture maintenance

Undifferentiated HepaRG® human hepatic cell line (BIOPREDIC, France; isolated from the female donor), also considered a surrogate for primary human hepatocytes (Guillouzo et al., 2007), was cultured in the basal hepatic cell medium supplemented with HepaRG® Growth Medium Supplement with antibiotics (BIOPREDIC, France). Cells were grown in T75 cell culture flasks until reaching 100 % confluency (usually 3–4 days). Later, cells were maintained in the same culture flask for an additional 14 days in order to promote differentiation into hepatocyte-like and biliary-like cells under DMSO-free conditions (Rose et al., 2022). Complete cell medium was changed every 2–3 days. The cells were maintained at 37 °C with 5 % CO_2 atmosphere.

2.3. Cell seeding, exposure, and sample collection

On day 1, cells were trypsinized and seeded in 24-well culture plates (VWR, Sweden) at the high density of 10^6 cells per well in the volume of 1000 μL and incubated for an additional 24 h. On day 2, cell media was removed and cells were exposed to perfluorohexyloctane (F6H8) in 500 μL of fresh media using five concentrations selected to approximate estimated systemic levels corresponding to 1-, 7-, 14-, 21-, and 28-day eyedrop use (D1, D7, D14, D21, and D28, respectively). F6H8 is a pure liquid and was added directly to the culture medium without any solvent or carrier. For each exposure level, the required volume of F6H8 was pipetted into a separate well of a 12-well plate containing fresh medium, mixed thoroughly by pipetting up and down 10–15 times, and immediately transferred onto the HepaRG cells. Control wells received fresh medium without F6H8 and were handled identically. The rationale for the selected concentrations was based on an estimated exposure model. We assumed that approximately 5 % of the administered ophthalmic dose could reach hepatic tissue. As per clinical usage, eye drops are typically prescribed up to four times per day, with one drop per administration. Given that a single drop contains approximately 11 μL of solution, this results in a total daily dose of 44 μL. Applying the 5 % systemic availability assumption, we estimated hepatic exposure and calculated equivalent concentrations for use in the in vitro model. The final concentrations applied in the 500 μL exposure volume were 0.44 %, 3.08 %, 6.16 %, 9.24 %, and 12.32 % v/v F6H8 for the D1, D7, D14, D21, and D28 groups, respectively. The 24-hour exposure was selected to enable stable metabolomic measurements, and the concentration series reflects estimated systemic levels rather than chronic exposure duration. After 24-h exposure, 300 μL of the cell culture supernatant was aspirated and transferred to a 96-deepwell microplate. The remaining cell media was removed and 300 μL of pre-warmed PBS was added on top of cells. Cells were gently detached by the cell scraper and transferred to a 96-deepwell microplate. Samples were stored at −80 °C until extraction and analysis. For each cell line, experiments included 4 technical replicates, and 3 independent experiments/biological replicates, yielding in total 12 replicates for each exposure condition.

2.4. Cell viability assessment

HepaRG cells were seeded at high density in 96-well black-walled microplates (Revvity) at 50,000 cells/well and incubated at 37 °C with 5 % CO_2 for 24 h. Afterwards, the medium was removed by inverting the plates, and the cells were exposed to the same concentrations of perfluorohexyloctane as described in the section *Cell seeding, exposure, and sample collection*. After 24 h of exposure, the alamarBlue assay was performed as described previously (Alijagic et al., 2023). In brief, the cell medium was removed, and 10 % alamarBlue™ HS Cell Viability Reagent (Invitrogen; Thermo Fisher Scientific, Eugene, OR, USA) in pre-warmed basal hepatic cell medium was added. The cells were incubated for 3 h at 37 °C. Fluorescence was then measured using a multi-mode microplate reader (FLUOstar Omega, BMG LABTECH, Ortenberg, Germany) at 540/590 nm excitation/emission. Viability is expressed as relative fold change compared to the negative (unexposed)

control (Supplementary Fig. 2).

2.5. Analysis of lipids, polar and semipolar metabolites

All samples were randomized before sample preparation and analysis. The samples were analyzed using two parallel methods, one aimed at analysis of polar and semipolar metabolites and the second one for the analysis of molecular lipids (Table 1). The cell pellets were first homogenized by adding 150 μL 0.9 % NaCl solution, after which the samples were vortex mixed and ultrasonicated for 3 min. Both analyses were done by an ultra-high-performance liquid chromatography quadrupole time-of-flight mass spectrometry (UHPLC-QTOFMS). In short, the UHPLC system used for lipidomic analyses was a 1290 Infinity II system from Agilent Technologies (Santa Clara, CA, USA. MassHunter B.06.01 software was used for data acquisition. For the analysis of polar and semipolar compounds, analyzed using an Xevo G3 QTOF system (Waters Corporation, Milford, Massachusetts, USA). The data acquisition was done using MassLynx V.4.2 (Waters Corporation).

80 μL of cell homogenate or 80 μL cell media was extracted with 480 μL of monophasic MeOH:MTBE:IPA (20:15:15, v/v) containing the following internal standards: Valine-d8, Glutamic acid-d5, Succinic acid-d4, Heptadecanoic acid, Lactic acid-d3, Citric acid-d4. 3-Hydroxybutyric acid-d4, Arginine-d7, Tryptophan-d5, Glutamine-d5, CA-d4, CDCA-d4, CDCA-d4, GCA-d4, GCDCA-d4, GLCA-d4, GUDCA-d4, LCA-d4, TCA-d4, UDCA-d4, 1,2-diheptadecanoyl-*sn*-glycero-3-phosphoethanolamine (PE(17:0/17:0)), N-heptadecanoyl-D-*erythro*-sphingosylphosphorylcholine (SM(d18:1/17:0)), N-heptadecanoyl-D-*erythro*-sphingosine (Cer(d18:1/17:0)), 1,2-diheptadecanoyl-*sn*-glycero-3-phosphocholine (PC(17:0/17:0)), 1-heptadecanoyl-2-hydroxy-*sn*-glycero-3-phosphocholine (LPC(17:0)) and 1-palmitoyl-d31-2-oleoyl-*sn*-glycero-3-phosphocholine (PC(16:0/d31/18:1)), and triheptadecanoylglycerol (TG(17:0/17:0/17:0)). After vortex-mixing (30 s), the extract was kept on an ice plate (45 min) and was filtered using filtration plates (0.45 μm). For polar/semipolar metabolite analysis, a 100 μL-aliquot was transferred to a vial, evaporated in a speed-vac system, and reconstituted with 50 μL MeOH:H_2O (7:3, v/v) for analysis. For lipidomics analysis, the extracted sample was directly anayzed with no additional step.

Quantitation was done using 6-point calibration (bile acids c = 20–640 ng/mL, polar metabolites c = 0.1 to 80 μg/mL). Quantification of other bile acids was done using the following compounds: CDCA, CA, DCA, GCDCA, GCA, GDCA, GHCA, GHDCA, GLCA, GUDCA, HCA, HDCA, LCA, αMCA, TαMCA, TβMCA, TCDCA, TCA, THCA, TDCA, THDCA, TLCA, and TωMCA. Polar metabolites were quantified by using alanine, citric acid, fumaric acid, glutamic acid, glycine, lactic acid, malic acid, 2-hydroxybutyric acid, 3-hydroxybutyric acid, linoleic acid, oleic acid, palmitic acid, stearic acid, cholesterol, fructose, glutamine, indole-3-propionic acid, isoleucine, leucine, proline, succinic acid, valine, asparagine, aspartic acid, arachidonic acid, glycerol-3-phosphate, lysine, methionine, ornithine, phenylalanine, serine, and threonine. The calibration curves had R values > 0.98 for most of the compounds. For lipidomics, calibration curves using 1-hexadecyl-2-(9Z-octadecenoyl)-*sn*-glycero-3-phosphocholine (PC(16:0e/18:1(9Z))), 1-(1Z-octadecenyl)-2-(9Z-octadecenoyl)-*sn*-glycero-3-phosphocholine (PC(18:0p/18:1(9Z))), 1-stearoyl-2-hydroxy-*sn*-glycero-3-phosphocholine (LPC(18:0)), 1-oleoyl-2-hydroxy-*sn*-glycero-3-phosphocholine (LPC(18:1)), 1-palmitoyl-2-oleoyl-*sn*-glycero-3-phosphoethanolamine (PE(16:0/18:1)), 1-(1Z-octadecenyl)-2-docosahexaenoyl-*sn*-glycero-3-phosphocholine (PC(18:0p/22:6)) and 1-stearoyl-2-linoleoyl-*sn*-glycerol (DG(18:0/18:2)), 1-(9Z-octadecenoyl)-*sn*-glycero-3-phosphoethanolamine (LPE(18:1)), N-(9Z-octadecenoyl)-sphinganine (Cer(d18:0/18:1(9Z))), 1-hexadecyl-2-(9Z-octadecenoyl)-*sn*-glycero-3-phosphoethanolamine (PE(16:0/18:1)) from Avanti Polar Lipids, 1-Palmitoyl-2-Hydroxy-*sn*-Glycero-3-Phosphatidylcholine (LPC(16:0)), 1,2,3 trihexadecanoalglycerol (TG(16:0/16:0/16:0)), 1,2,3-trioctadecanoylglycerol (TG(18:0/18:0/18:0) and 3β-hydroxy-5-cholestene-3-stearate (ChoE(18:0)), 3β-Hydroxy-5-cholestene-3-linoleate (ChoE(18:2)) from Larodan, were prepared to the following concentration levels: 100, 500, 1000, 1500, 2000 and 5000 ng/mL (in CHCl3:MeOH, 2:1, v/v) including 1250 ng/mL of each internal standard. The curves had R values > 0.99 for all lipids. Identification was done based on *in-house* library (*m/z*, MS/MS, retention times) that is based on analysis of authentic standards. Lipid abbreviations are as follows: lipid headgroup followed by the fatty acyl composition (number of carbons in the fatty acyl, number of double bonds). Lipid headgroups: ceramide (Cer), sphingomyelin (SM), phosphatidylcholine (PC), alkylphosphatidylcholine (PC-O), phosphatidylcholine plasmalogen (PC-P), lysophosphatidylcholine (LPC), phosphatidylethanolamine (PE), akylphosphatidylethanolamine (PE-O), phosphatidylethanolamine plasmalogen (PE-P), lysophosphatidylethanolamine (LPE), phosphatidylinositol (PI), phosphatidylserine (PS), cholesterol ester (CE), diacylglycerol (DG), triacylglycerol (TG).

Standard solutions extracted blanks (n = 3), pooled QC samples (n = 3, an aliquot of each sample pooled), in-house serum QC and NIST SRM 1950 (human plasma) were analyzed together with the samples. Identification was done based on in-house library with retention time and spectral data (level 1 identification, based on Metabolic Standard Initiative (Sumner et al., 2007) and based on MS spectra using on-line spectral libraries (level 2 identification). For pooled samples, identified lipids had an average RSD in the pooled cell samples 15.1 % and in extracellular media RSD was on average 16.8 %. For polar and semipolar compounds, the RSDs were 25.1 % and 26.5 % for cells and extracellular media, respectively.

Additionally, we applied UHPLC fractionation system (Waters Corporation, Milford, Massachusetts, USA) for isolation and concentration of the putative biotransformation product, using the same chromatographic conditions as above, and using fractionation windows of ± 0.5 min of the actual retention time (5.67 min) and collecting the fraction from 5 repetitive analyses. The fraction was then analyzed and the CCS value of the compound was measured using the identical chromatographic conditions using the same Waters UHPLC system as above coupled to the Bruker timsTOF flex system (Bruker timsTOF, Bruker Daltonik, Bremen, Germany). The instrument was set up to run in prmPASEF negative mode with an MS1 scan of 0.1 ms and a Q1 set to 461.0781 for the PASEF scans. The prm window was defined for the whole MS run. The source settings were as follows: ion spray voltage of −3600 V, dr gas at 10 L/min, dry temperature at 220 degrees, The ion mobility ramp was set between 0.55 V.s/cm^2 and 1.90 V.s/cm^2 and ramped over 100 ms with an accumulation time of 100 ms. The MS was scanned between 100 and 1350 *m/z*. The instrument was mass calibrated using sodium formate and the mobility calibrated using the Agilent ESI tune mix (positive). The ion mobility was determined by manual inspection of the data an matching the MS2 spectra in Data Analysis (Bruker).

2.6. Data preprocessing

Processing of MS data was performed using the open-source software package MZmine 4.5.0 (Schmid et al., 2023). The following steps were applied in this processing: (i) Crop filtering with a *m/z* range of 350 – 1200 *m/z* and an RT range of 2.0 to 12 min, (ii) Mass detection with a noise level of 750 for MS 1 and 200 for MS 2 level, (iii) Chromatogram builder with a minimum time span of 0.08 min, minimum height of 1000 and a *m/z* tolerance of 0.006 *m/z* or 10.0 ppm, (iv) Chromatogram deconvolution using the local minimum search algorithm with a 70 % chromatographic threshold, 0.05 min minimum RT range, 5 % minimum relative height, 1200 minimum absolute height and minimum ration of peak top/edge of 1.2, (v) Isotopic peak grouper with a *m/z* tolerance of 5.0 ppm, RT tolerance of 0.05 min, maximum charge of 2 and with the most intense isotope set as the representative isotope, (vi) Join aligner with a *m/z* tolerance of 0.009 or 10.0 ppm and a weight for of 2, a RT tolerance of 0.15 min and a weight of 1 and with no requirement of charge state or ID and no comparison of isotope pattern,

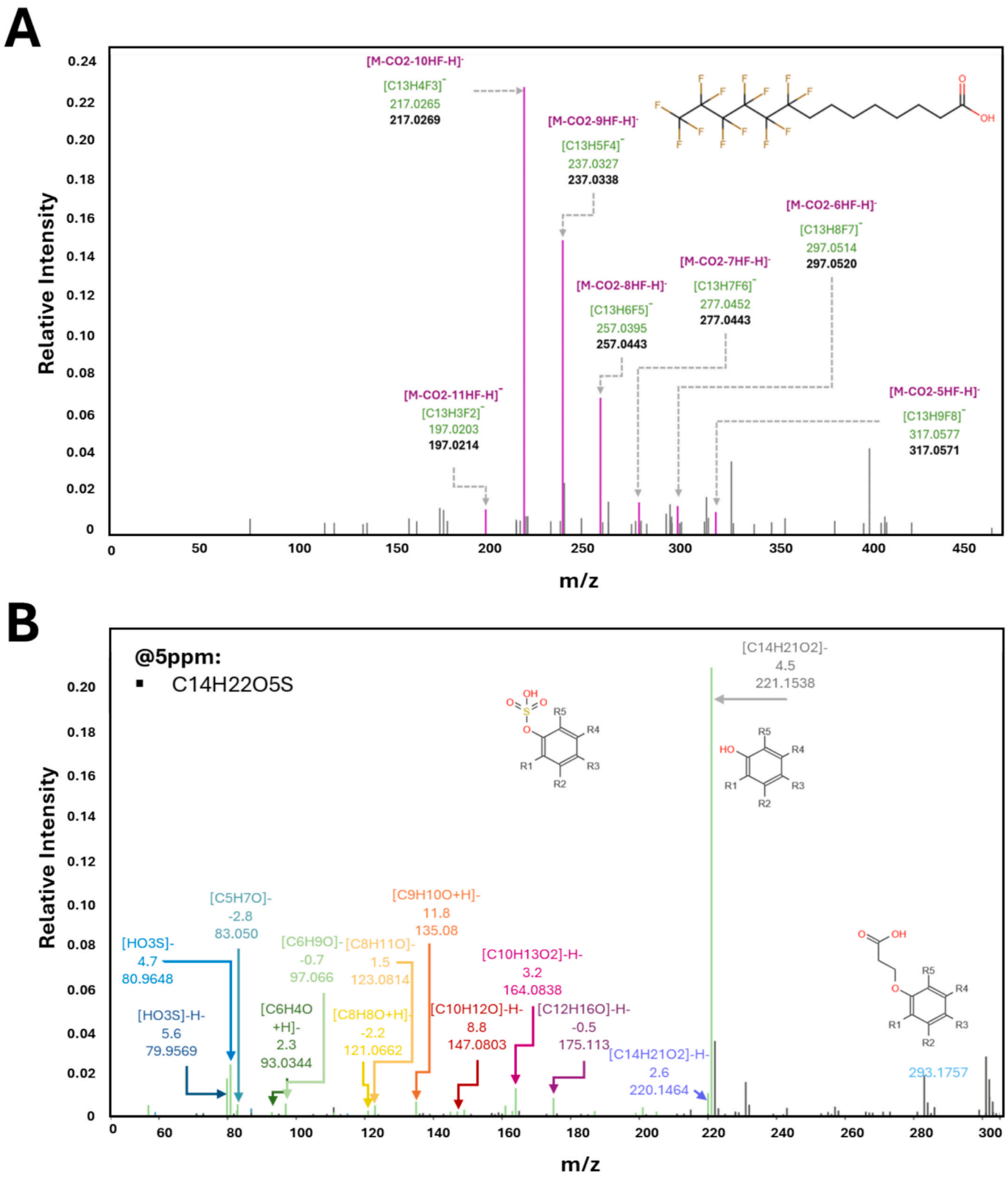

Fig. 1. (A) MS/MS spectrum of Compound 66 (m/z = 461.0781, rt 5.67 min) in cells was linearly correlating with the F6H8 exposure concentration (R = 0.78, p = $1.81e^{-18}$, FDR = $1.94e^{-16}$). (B) MS/MS spectrum of Compound 203 (m/z = 301.1103, rt 2.98 min) in cells was linearly correlating with the F6H8 exposure concentration (R = 0.89, p = 1.59^{-29}, FDR = $3.4e^{-27}$).

(vii) Peak list row filter with a minimum of 10 % of the samples (viii) Gap filling using the same RT and m/z range gap filler algorithm with an m/z tolerance of 0.009 m/z or 10.0 ppm, (ix) Identification of lipids and metabolites using a custom database search with an m/z tolerance of 0.007 m/z or 8.0 ppm and a RT tolerance of 0.25 min, and (x) Normalization using internal standards: For lipids: PE(17:0/17:0), SM (d18:1/17:0), Cer(d18:1/17:0), LPC(17:0), TG(17:0/17:0/17:0) and PC (16:0/d30/18:1)) for identified lipids and closest internal standard for

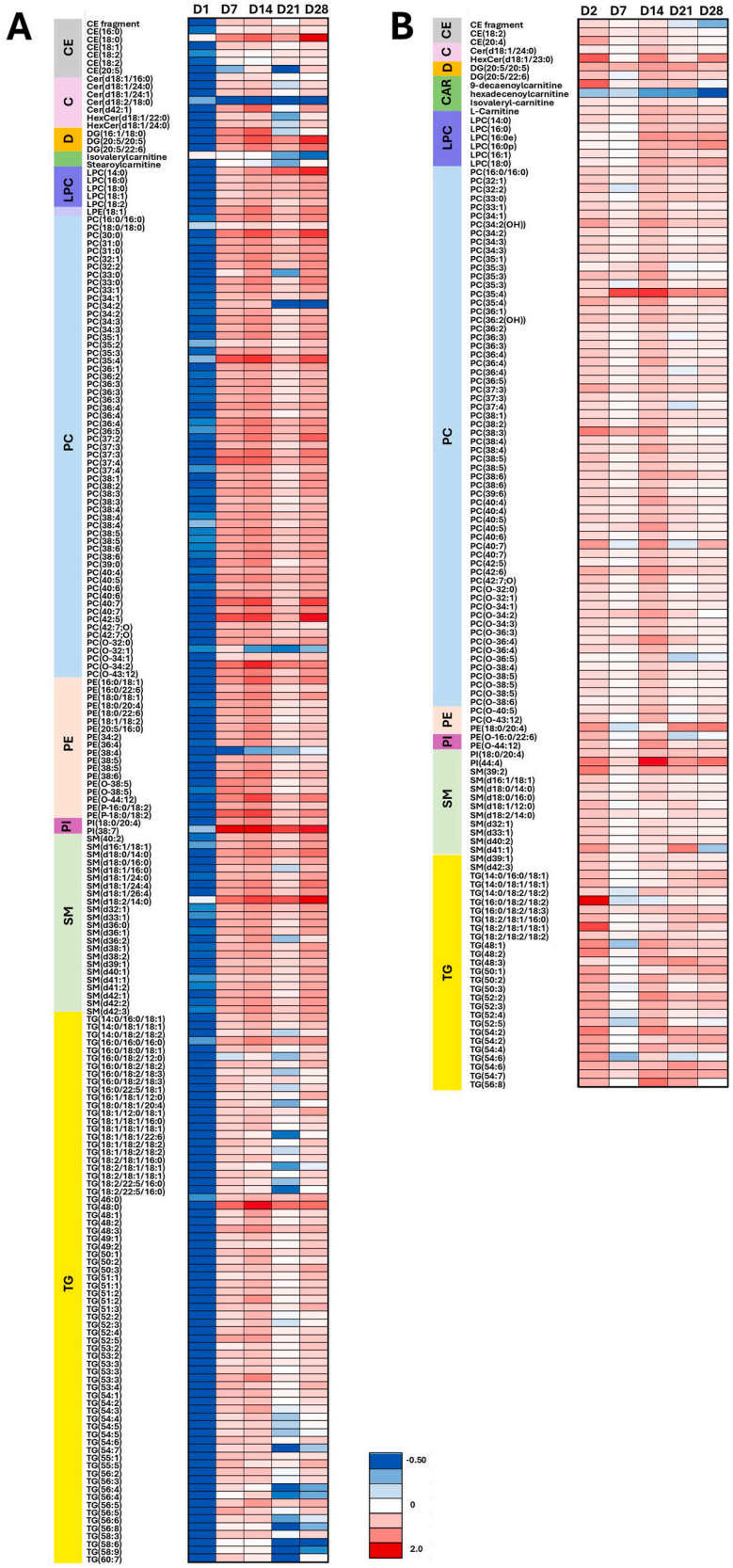

Fig. 2. Fold changes in lipids levels between F6H8-exposed and control HepaRG cells across different exposure concentrations, shown for both (A) cells and (B) extracellular media. Only those fold changes that are significant at least in one exposure concentration are shown. Lipid class abbreviations: CE – cholesteryl ester, Cer – ceramide, LPC – lysophosphatidylcholine, PC – phosphatidylcholine, PI – phosphatidyl inositol, PE – phosphatidylethanolamine, SM – sphingomyelin, TG – triacylglycerol, DG – diacylglycerol.

the unknown lipids followed by calculation of the concentrations based on lipid-class concentration curves. For polar metabolites the following internal standards were used: valine-d8, glutamic acid-d5, succinic acid-d4, heptadecanoic acid, lactic acid-d3, citric acid-d4. 3-hydroxybutyric acid-d4, arginine-d7, tryptophan-d5, glutamine-d5, CA-d4, CDCA-d4, GCA-d4, GCDCA-d4, GLCA-d4, GUDCA-d4, LCA-d4, TCA-d4, UDCA-d4 and closest internal standard for the unknown metabolites followed by calculation of the concentrations-based concentration curves. For data filtering, we have removed compounds that were present at blank samples (peak area $>$ 5 times that of blank) and compounds that had RSD $>$ 30 % in the pooled quality control samples. MS/MS data was done for the pooled quality control samples using auto MS/MS mode. The two cell lines were analyzed separately but the data preprocessing was done together. The data was adjusted by in-house pooled samples that were analyzed in both batches to correct the difference between the two batches.

2.7. Data analysis

Data analyses were conducted using MetaboAnalyst 6.0 (Pang et al., 2024) and the R statistical programming language (version 4.1.2) (https://www.r-project.org/). In order to correct for heteroscedasticity, the exposure datasets were pre-processed by log10 transformation and scaling to zero mean and unit variance (autoscaled) as metabolomics data is not normally distributed. The statistical analyses included principal component analysis (PCA), analysis of variance (ANOVA), *t*-test and fold-change between controls and each exposure concentration, Spearman correlations between the biotransformation product and metabolites.

Pathway enrichment analysis was performed using the MetaboAnalyst 6.0 web platform with the Functional Analysis (MS Peaks) module (Lu et al., 2022). This approach supports functional analysis of untargeted metabolomics data generated from high-resolution mass spectrometry. The pathway analysis was done with the data of the polar and semipolar metabolites, as the pathway analysis for lipidomics data is not sufficiently robust due to lack of exact structures of the lipids (fatty acid composition, including the position of the double bonds, cis/trans configuration). However, our polar/semipolar panel (Method 1) includes a large number of lipids, except for neutral lipids (CE, DG, TG) that are not covered either by sample preparation nor the negative ion mode. The input data for the pathway analysis comprised complete LC-HRMS data, *i.e.*, both identified and unknown metabolites, obtained in negative ionization mode. First, we performed statistical analyses using *t*-test between control and each exposure concentration between F6H8 and polar metabolites and lipids, resulting in fold change, p values and FDR values. Additionally, we analysed Spearman correlation between the biotransformation product and with the metabolites. The whole input peak list, with peak names given as their numeric mass (*m/z*) values for putative annotation, and the statistical results with p-values and t-score or correlation was used for the pathway analysis. Two algorithms were applied separately, namely, Mummichog and Gene Set Enrichment Analysis (GSEA) and two pathway libraries were used in the pathway analysis, namely human scale metabolic model MNF (from MetaboAnalyst Mummichog package) and Kyoto Encyclopedia of Genes and Genomes (KEGG) pathways for *Homo Sapiens* to determine the relative significance of the identified pathways (Li et al., 2013). In addition, targeted pathway analyses were performed for the biotransformation product. The mass tolerance for the pathway analysis was set at 7 ppm, and we also used an advanced option to select representative adducts by removing isotopic adducts as these have been already removed in our data preprocessing step.

3. Results

3.1. Global metabolic responses to perfluorohexyloctane exposure

To evaluate the metabolic effects of F6H8, we performed comprehensive metabolomic analysis including lipidomic profiling of both hepatocytes and their extracellular environment across a wide range of non-cytotoxic exposure concentrations.

We observed a strong linear relationship with F6H8 concentration and with several compounds, both in the cells as well as in the extracellular media (**Supplementary Table 1**). Notably, three unknown compounds in both cells and media showed a very strong ($R > 0.78$, FDR $< 1.9e^{-16}$) correlation with the exposure concentration, and these compounds were not detected in control cells nor in control media. For two of the compounds, we could obtain mass spectra. Based on MS/MS spectra, one of these compounds could be a derivative of F6H8, *i.e.*, F6H8 biotransformation product. The compound was identified as a carboxylic-acid derivative of F6H8, namely perfluorohexyloctanoic acid (Fig. 1A). The deprotonated molecular ion, $[M-H]^-$, matched that of perfluorohexyloctanoic acid with a mass error < 1 ppm. In the negative-ion MS/MS spectrum, the product ions arise from neutral loss of the carboxyl group and from sequential, extensive HF eliminations. This loss pattern has previously been observed both on H-substituted PFAS (*e.g.*, fluorotelomer carboxylic acids) (Wang et al., 2024; Zweigle et al., 2022) and semi-fluorinated alkanes (Napoli et al., 1993). In addition to the mass spectral data, also the retention time (rt) of the compound (5.67 min) was in line with the corresponding fully fluorinated carboxylic acid (perfluoro-n-tetradecanoic acid, rt = 5.74 min) which had a slightly higher retention time than partially fluorinated compound. We also performed a retention time prediction, based on the logP value of perfluorohexyloctanoic acid, computed to be 6.9 according to Pubchem model XlogP3 3.0 (**Supplementary Fig. 3**). Using the linear regression equation, the predicted retention time of the compound is 5.77 min, which is very close to the retention time measured, with $\Delta rt = 0.07$ min. The compound was further isolated using LC fractionation and analyzed by UHPLC coupled to ion mobility time-of-flight mass spectrometry (IM–TOFMS) (**Supplementary Fig. 4**). The experimentally determined mobility value was 0.883 V·s/cm^2, corresponding to a collision cross section (CCS) of 182.3 Å^2. According to the AllCCS2 model (https://doi.org/10.1038/s41467-020–18171-8), perfluorohexyloctanoic acid is predicted to have a CCS value of 173.5 Å^2, representing a 4.8 % deviation from the experimental value. The second unknown compound of interest showed a typical fragment of sulfonic group (Fig. 1B), and co-clustered with other sulphate containing metabolites in ion network analysis. However, majority of the compounds that correlated with the F6H8 concentration could not be identified.

Overall, 65 polar/semipolar compounds and 66 lipids showed significant correlation (FDR < 0.05) with F6H8 concentration, among which 23 were negatively and the remainder positively correlated. Of the identified compounds, several free fatty acids (FFAs) were negatively associated with the exposure as well as one amino acid, one acylcarnitine, and two lipids. Large number of lipids, amino acids, two bile acids, and some sugar derivatives were positively correlated with the F6H8 concentration.

3.2. Lipidome alterations in hepatocytes and extracellular media

As we observed that the exposure to F6H8 caused concentration-dependent, non-monotonic changes, we next investigated the impact of exposure on each induvial concentration level, compared to the control samples, as indicated by fold changes relative to the controls (Fig. 2, **Supplementary Tables 4–5**). In the extracellular media, The exposure caused a clear increase of lipids, except for hexadecenoylcarnitine, which was downregulated. Particularly phospholipids and several TGs were upregulated in the media, and both lysophospholipids and PC(35:4) exhibited increasing upregulation with

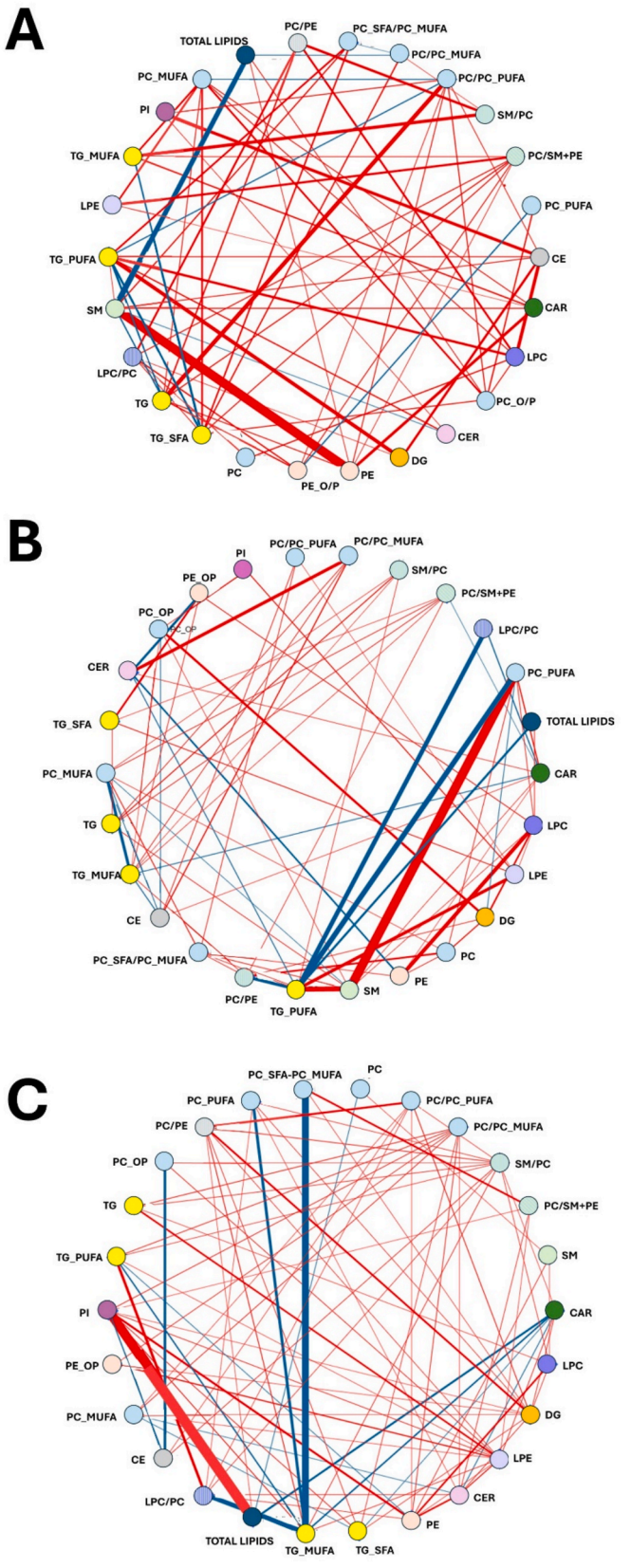

(caption on next column)

Fig. 3. Partial correlation networks including lipid classes as node, in (A) control HepaRG cells, (B) cells exposed to the lowest F6H8 concentration, and (C) cells exposed to the highest F6H8 concentration. The networks illustrate reduced interclass connectivity between lipid species following exposure. The thickness of lines represents the strength of correlation, with red lines representing positive correlation, and blue lines negative correlation. Lipid class abbreviations: CE – cholesteryl ester, LPC – lysophosphatidylcholine, PC – phosphatidylcholine, PI – phosphatidyl inositol, PE – phosphatidylethanolamine, SM – sphingomyelin, TG – triacylglycerol, DG – diacylglycerol. For phospholipids, OP states alkylether derivatives of parent phospholipid, for TGs and phospholipids, SFA defines saturated fatty acyls, MUFA monounsaturated fatty acyls and PUFA polyunsaturated fatty acyls.

higher F6H8 concentrations. We also observed dose-dependent increase in polyunsaturated FFAs, while the saturated FFAs were downregulated with increasing F6H8 exposure.

In cells, there was even more substantial effect on lipid profiles, with the lowest F6H8 concentration causing marked reduction of large number of lipids, with inverse trend at the higher exposures, with several lipids upregulated following exposure. For example, ceramide Cer(d18:2/18:0) was consistently downregulated at all tested concentrations, while sphingomyelin SM(d18:2/14:0) was upregulated at the higher exposure levels, but not at lower exposure levels.

Given the widespread lipid alterations, we also investigated the impact of exposure on the level of lipid classes and lipid class ratios. Lysophosphatidylcholines (LPCs) and (PC phosphatidylcholine (PC) ratio (LPC/PC) had a significant positive correlation with the exposure concentration. We also performed partial correlation analysis across the exposure groups for the lipid classes, comparing the correlation patterns in control cells and exposed cells (Fig. 3). Marked positive correlations observed between different lipid classes in control cells were altered following the exposure to F6H8, with less intra-class positive correlations and strong negative correlations between polyunsaturated fatty acid (PUFA)-containing TGs and (i) LPC/PC and PC_PUFA at the lowest exposure concentration. and (ii) monounsaturated fatty acids (MUFA) containing TG and saturated fatty acids (SFA) containing PCs at the highest F6H8 concentration. Also, the association between phosphatidylethanolamines (PEs) and SMs was lost after the F6H8 exposure.

3.3. Effects on polar and semipolar metabolite profiles

We also investigated the impact of exposure on polar and semipolar metabolites at each concentration level separately. Similarly as for lipids, we observed concentration-dependent, non-monotonic changes both in cells and extracellular media (Fig. 4, Supplementary Tables 2–3). In cells, four amino acids (5-oxoproline, aspartic acid, ketoleucine, and threonine) were significantly altered, with varying pattern of changes. Aspartic acid and ketoleucine were downregulated at higher F6H8 exposure concentrations, with no significant changes at lower exposure levels. Among FFAs, three were significantly affected, with eicosatetraenoic acid showing a linear decrease with the increasing F6H8 concentration. In the extracellular media, FFAs showed patterns that were linked with their saturation level: saturated FFAs were downregulated while mviabioityonounsaturated (MUFA) and polyunsaturated (PUFA) fatty acids were upregulated, particularly at the highest concentration. Amino acids and their derivatives generally exhibited a downregulation trend.

3.4. Pathway enrichment and functional analysis

We also performed both lipid enrichment and functional analysis at the pathway level for the lowest and highest F6H8 concentrations, which showed opposite metabolic patterns (Table 2). Four pathways were affected at both concentrations (Biosynthesis of unsaturated fatty acids, Fatty Acid Metabolism, Chondroitin sulfate degradation and Heparan sulfate degradation) but showed opposite trends: all were

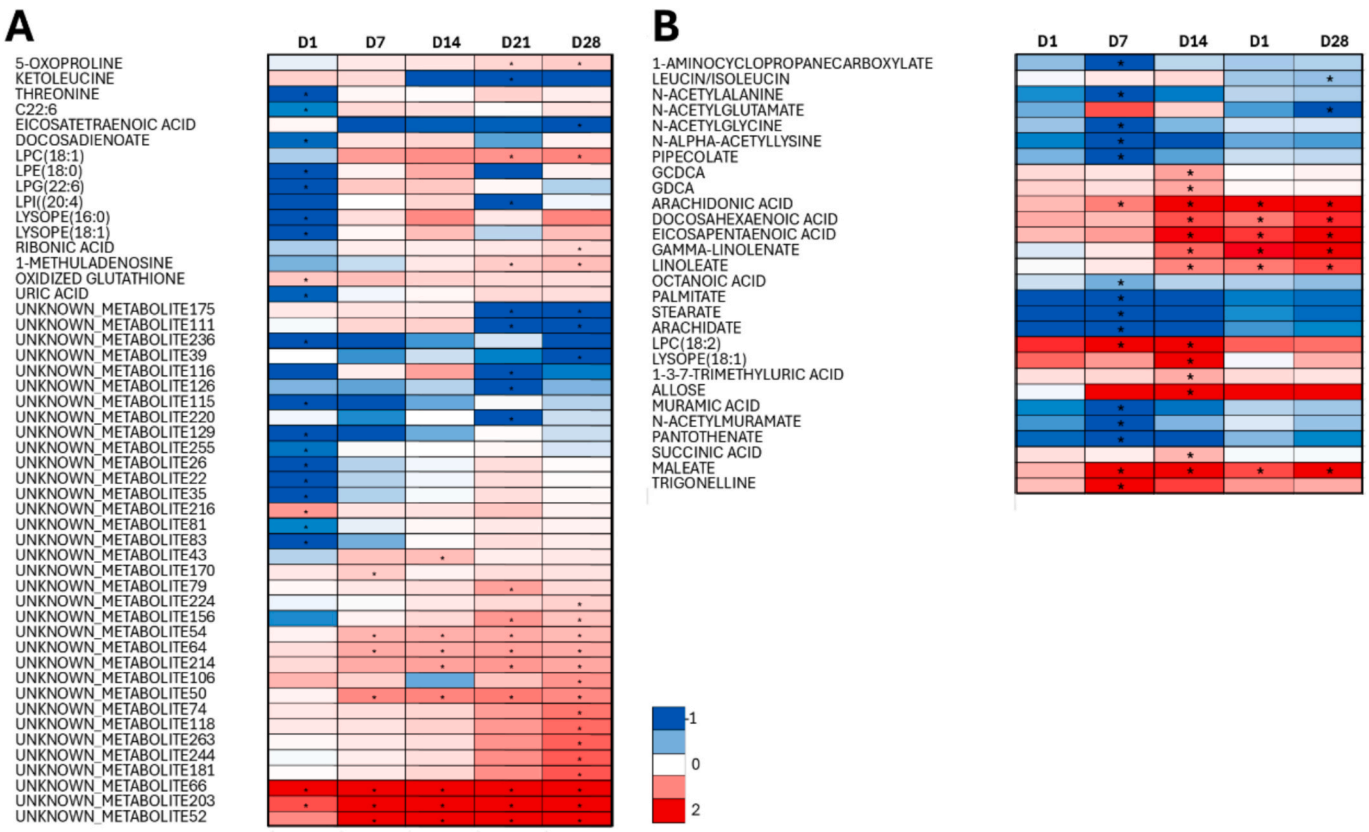

Fig. 4. Fold changes in polar/semipolar metabolites between F6H8-exposed samples and control cells and across different exposure concentrations in (A) HepaRG cells, and (B) in extracellular media. Only those fold changes that are significant at least in one exposure level are shown. For extracellular media, only identified compounds are shown. For detailed information, see Supplementary Table 3.

downregulated at the lowest concentration and upregulated at the highest. At the lowest F6H8 concentration, a large number of pathways related to fatty acid and lipid metabolism were altered as well as pathways related to amino acid and nitrogen metabolism. Majority of the affected pathways were downregulated, only Keratan sulfate biosynthesis was upregulated at the lowest exposure concentration. Notably, sphingolipid metabolism was among the most prominently affected pathways. At the highest F6H8 concentration, alterations were observed in several amino acids and nitrogen metabolism-related pathways, along with some fatty acid related pathways. In addition, the metabolic pathways linked with central carbon metabolism were also affected. Central carbon and energy metabolism related pathways were mainly downregulated while amino acids and nitrogen metabolism-related pathways showed alteration in both directions, indicating complex regulatory responses at higher exposure levels.

3.5. Biotransformation product, perfluorohexyloctanoic acid, is associated with metabolic alterations

We next examined whether the biotransformation product, perfluorohexyloctanoic acid, was associated with the metabolic patterns of HepaRG cells or the extracellular medium. We found significant correlations between this metabolite and more than 280 identified polar and semipolar metabolites, as well as lipids, within the cells, and with 67 metabolites in the culture medium (Supplementary Tables 4 and 5). This represents roughly a sevenfold increase in the number of metabolites correlated with the biotransformation product compared with the parent compound. In the cells, several amino acids and three conjugated bile acids showed positive correlations with perfluorohexyloctanoic acid, whereas two amino acids (ketoleucine and tryptophan) were negatively correlated. Most free fatty acids and lipid species also exhibited positive correlations. In the culture medium, five acylcarnitines and octanoic acid were negatively correlated with the metabolite, while all other detected metabolites, including L-carnitine, showed positive correlations.

Based on pathway analysis (Table 3), the main metabolic pathways dysregulated in response to increasing concentrations of this compound included nitrogen-related amino acid metabolism (arginine and urea cycle pathways; alanine, aspartate and glutamate metabolism), pathways linked to mitochondrial flux (glyoxylate and dicarboxylate metabolism; purine metabolism), and pathways involving lipid and bile acid metabolism.

4. Discussion

In this study, we observed pronounced metabolic alterations in F6H8-treated human hepatocytes. The choice of hepatocytes and the exposure design were guided by evidence that structurally related hydrophobic alkanes and semifluorinated hydrocarbons preferentially accumulate in the liver and exhibit prolonged hepatic retention, with half-lives extending over several weeks in animal models (Zarif et al., 1994; Cravedi and Tulliez, 1986; McCarthy, 1964; Tulliez and Bories, 1978). This supports the liver as a biologically plausible target organ for systemic F6H8 exposure, despite its primary ocular route of administration. Exposure concentrations were therefore selected to approximate estimated hepatic burdens arising from repeated ophthalmic use rather than acute systemic dosing. Importantly, this rationale is further supported by recent regulatory evidence. The U.S. Food and Drug Administration's *Report on the Use of PFAS in Cosmetic Products and Associated Risks* (2026) notes that perfluorohexane that was previously considered biologically inert, exhibited evidence of metabolic transformation in liver-based test systems, challenging the assumption that fluorinated

Table 2
Summary of pathway enrichment analysis for the lowest (ED1) and highest (ED28) F6H8 exposure concentrations. Pathways showing significant enrichment ($p < 0.05$) are listed along with their direction of change.

Comment	Pathway	ED1	p ED1	ED28	p ED28
Amino Acid & Nitrogen Metabolism	Beta-alanine degradation I	ns		up	0.011
Amino Acid & Nitrogen Metabolism	Aminosugars metabolism	down	0.039	ns	
Amino Acid & Nitrogen Metabolism	Arginine and proline metabolism	ns		up	0.028
Amino Acid & Nitrogen Metabolism	Citrulline biosynthesis	down	0.022	ns	
Amino Acid & Nitrogen Metabolism	Glutamate metabolism	ns		down	0.042
Amino Acid & Nitrogen Metabolism	Glycine, serine and threonine metabolism	ns		down	0.031
Amino Acid & Nitrogen Metabolism	Methionine and cysteine metabolism	ns		down	0.049
Amino Acid & Nitrogen Metabolism	proline biosynthesis II (from arginine)	ns		up	0.009
Amino Acid & Nitrogen Metabolism	threonine degradation II	down	0.004	ns	
Amino Acid & Nitrogen Metabolism	Urea cycle/amino group metabolism	ns		up	0.044
Central carbon and energy metabolism	Butanoate metabolism	ns		up	0.029
Central carbon and energy metabolism	Citrate cycle (TCA cycle)	ns		down	0.029
Central carbon and energy metabolism	D-glucuronate degradation I	ns		up	0.009
Central carbon and energy metabolism	Glyoxylate and dicarboxylate metabolism	ns		down	0.024
Central carbon and energy metabolism	Propanoate metabolism	ns		down	0.025
Central carbon and energy metabolism	Pyruvate metabolism	ns		down	0.038
Lipid and fatty acid metabolism	Biosynthesis of unsaturated fatty acids	down	0.008	up	0.033
Lipid and fatty acid metabolism	De novo fatty acid biosynthesis	down	0.021	ns	
Lipid and fatty acid metabolism	Fatty acid activation	down	0.029	ns	
Lipid and fatty acid metabolism	Fatty Acid Metabolism	down	0.050	up	0.045
Lipid and fatty acid metabolism	Glycerolipid metabolism	ns		up	0.019
Lipid and fatty acid metabolism	Glycosphingolipid biosynthesis – ganglioseries	down	0.016	ns	
Lipid and fatty acid metabolism	Glycosphingolipid biosynthesis – globoseries	down	0.013	ns	
Lipid and fatty acid metabolism	Glycosphingolipid biosynthesis – lactoseries	down	0.031	ns	
Lipid and fatty acid metabolism	Glycosphingolipid biosynthesis – neolactoseries	down	0.045	ns	
Lipid and fatty acid metabolism	Glycosphingolipid metabolism	down	0.042	ns	
Lipid and fatty acid metabolism	leukotriene biosynthesis	down	0.004	ns	
Lipid and fatty acid metabolism	Leukotriene metabolism	down	0.024	ns	
Lipid and fatty acid metabolism	Linoleic acid metabolism	down	0.023	ns	
Lipid and fatty acid metabolism	Phosphatidylinositol phosphate metabolism	down	0.013	ns	
Lipid and fatty acid metabolism	Phytanic acid peroxisomal oxidation	ns		down	0.038
Glycosaminoglycan turnover	Chondroitin sulfate degradation	down	0.030	up	0.038
Glycosaminoglycan turnover	Heparan sulfate degradation	down	0.030	up	0.038
Glycosaminoglycan turnover	Hyaluronan Metabolism	down	0.017	ns	
Glycosaminoglycan turnover	Keratan sulfate biosynthesis	up	0.031	ns	
Glycosaminoglycan turnover	Keratan sulfate degradation	down	0.030	ns	
Protein glycosylation	N-Glycan biosynthesis	down	0.019	ns	
Protein glycosylation	O-Glycan biosynthesis	down	0.045	ns	
Cofactor and Vitamin Metabolism	Porphyrin metabolism	down	0.039	ns	
Cofactor and Vitamin Metabolism	Pyrimidine metabolism	down	0.025	ns	
Nucleotide and Translation Machinery	tRNA charging	down	0.026	ns	
Nucleotide and Translation Machinery	Vitamin B6 (pyridoxine) metabolism	down	0.045	ns	

hydrocarbons are universally resistant to biotransformation. In this context, our detection of a putative carboxylic acid derivative of F6H8 provides experimental support for the possibility that semifluorinated alkanes may undergo hepatic metabolism, supporting the relevance of hepatocyte-based models for evaluating their systemic biological effects. Indeed, we detected mass spectral features consistent with fluorinated metabolites in F6H8-treated hepatocytes, including a compound tentatively annotated as perfluorohexyloctanoic acid, suggesting oxidative biotransformation of F6H8. This observation aligns with previous studies showing that structurally analogous non-fluorinated saturated alkanes can undergo hepatic ω-oxidation to yield carboxylic acids of the same chain length. (Cravedi and Tulliez, 1986; McCarthy, 1964; Tulliez and Bories, 1978) The proposed alkane oxidation pathway in hepatocytes involves sequential cytochrome P450-mediated hydroxylation of the terminal methyl group to a primary alcohol, followed by oxidation to an aldehyde *via* alcohol dehydrogenase and subsequent conversion to the corresponding carboxylic acid by aldehyde dehydrogenase. Given the structural similarity to alkanes, F6H8 may undergo biotransformation through an analogous pathway. Although definitive structural confirmation was not possible due to the absence of analytical reference standards, the detection of fluorine-containing features challenges the assumption that semifluorinated alkanes are biologically inert and highlights the importance of considering downstream metabolites in safety assessments, as carboxylic acid derivatives are often more bioactive and persistent than their parent compounds.

Exposure to F6H8 resulted in marked alterations in lipid homeostasis, including elevated lipid levels in the extracellular medium across all concentrations. This pattern suggests enhanced lipid efflux or membrane

Table 3
Summary of pathway enrichment analysis and targeted pathway analyses associated with the biotransformation product levels in cells. Pathways showing significant enrichment ($p < 0.05$) are listed.

Approach	Pathway	p	Direction
targeted	Alanine, aspartate and glutamate metabolism	0.0158	upregulated
targeted	Alpha Linolenic Acid and Linoleic Acid Metabolism	0.0145	upregulated
targeted	Ammonia Recycling	0.0083	upregulated
targeted	Arginine biosynthesis	0.0021	upregulated
BIOCYC	Arginine biosynthesis IV	0.0109	upregulated
BIOCYC	Arginine degradation I (arginase pathway)	0.0118	upregulated
BIOCYC	Arginine degradation VI (arginase 2 pathway)	0.0111	upregulated
BIOCYC	Aspartate degradation II	0.0118	upregulated
BIOCYC	Bile acid biosynthesis, neutral pathway	0.0111	upregulated
targeted	Biosynthesis of unsaturated fatty acids	0.00004	upregulated
BIOCYC	Citrulline biosynthesis	0.0330	upregulated
targeted	Glycerophospholipid metabolism	0.00081	upregulated
targeted	Glyoxylate and dicarboxylate metabolism	0.0029	upregulated
KEGG, targeted	Histidine metabolism	0.00320	upregulated
targeted	Lysine degradation	0.0398	upregulated
targeted	Mitochondrial Beta-Oxidation of Long Chain Saturated Fatty Acids	0.0071	Acylcarnitines upregulated, saturated FFAs downregulated
KEGG	Primary bile acid biosynthesis	0.0225	upregulated
BIOCYC	Proline biosynthesis II (from arginine)	0.0220	upregulated
targeted	Purine metabolism	0.0440	upregulated
targeted	Sphingolipid metabolism	0.0006	upregulated
BIOCYC	Urea cycle	0.0333	upregulated

remodeling rather than simple intracellular accumulation. Semi-fluorinated alkanes are known to integrate into phospholipid bilayers and form phase-separated domains due to the lipophobic nature of their fluorinated chains, a process that can alter membrane fluidity, curvature, and protein function (Sabín et al., 2006; Ferro and Krafft, 2002). Such membrane perturbations provide a unifying mechanistic framework for the observed lipidomic changes, including altered phospholipid turnover, sphingolipid homeostasis, and mitochondrial membrane integrity.This response may additionally reflect F6H8-induced metabolic dysregulation, or indicate membrane perturbations that trigger remodeling, breakdown, or stress responses such as endoplasmic reticulum (ER) stress or oxidative stress. O Consistent with this interpretation, lysophospholipids displayed concentration-dependent, non-monotonic responses, with decreased intracellular levels at low concentrations and marked accumulation at higher exposures in both cells and media. This pattern may reflect altered phospholipase activity or impaired reacylation via the Lands' cycle, processes that are highly sensitive to membrane integrity and oxidative stress.. Concurrently, the consistent downregulation of acylcarnitines in both compartments suggests suppression of mitochondrial β-oxidation, potentially compromising energy metabolism and fatty acid homeostasis.

At the pathway level, F6H8 exposure induced concentration-dependent alterations in multiple metabolic pathways, many of which displayed non-monotonic responses. At the lowest concentration, affected pathways were primarily related to lipid signalling and inflammatory activation, including perturbations in sphingolipid, glycosphingolipid, and leukotriene metabolism. Sphingolipids are key regulators of cell proliferation, adhesion, migration, autophagy, apoptosis, and mitochondrial function (Apostolopoulou et al., 2018) and their dysregulation has been implicated in type 2 diabetes, metabolic syndrome, and drug-induced liver injury (Balram et al., 2022; Gai et al., 2023). At higher concentrations, disruption extended to central carbon metabolism and amino acid degradation pathways, indicating loss of metabolic compensation and broader cellular stress.

The non-monotonic dose–response patterns observed here align with reports for conventional PFAS in *in vitro*, *in vivo*, and human studies and are often interpreted within a hormetic framework (Rotander et al., 2024; Alijagic et al., 2024; Rotander et al., 2024; Labine et al., 2022; Kariuki et al., 2017; Geng et al., 2019; Andi Alijagic et al., 2024). At lower exposure levels, adaptive responses may preserve cellular homeostasis, whereas higher exposures overwhelm compensatory mechanisms (Kim et al., 2018; Rossnerova et al., 2020). (Kim et al., 2018) For membrane-active compounds such as F6H8, such biphasic behavior may reflect threshold effects associated with membrane buffering capacity and cumulative lipid perturbation.

Notably, the biotransformation product exhibited broader and stronger metabolic associations than the parent compound, suggesting that even limited conversion of F6H8 may substantially amplify biological effects. This observation aligns with the behavior of other fluorinated carboxylic acids, which exhibit higher bioactivity and persistence than their neutral precursors. Pathway analysis revealed both shared and distinct effects compared with F6H8, with the metabolite uniquely affecting purine metabolism, bile acid metabolism, and nitrogen-handling pathways. These findings suggest that even limited metabolic conversion of F6H8 may substantially alter its biological impact, reinforcing the need to consider metabolite-mediated effects when evaluating semifluorinated compounds. Some differences between the metabolite and parent compound may also reflect methodological factors: the biotransformation product was analyzed using correlation across the full dataset, whereas the parent compound was evaluated concentration by concentration. Non-monotonic responses in certain metabolites mean that these approaches can highlight different biological signals. Thus, the observed divergence in pathway profiles likely reflects both true biological differences and the influence of the analytical strategy used.

Comparison with conventional PFAS highlights both similarities and differences. While PFAS exposure is typically associated with suppression of bile acids and acylcarnitines through receptor-mediated mechanisms such as CYP7A1 inhibition, F6H8 predominantly affected lipid and amino acid metabolism with minimal bile acid disruption. This suggests that F6H8 acts primarily through membrane-associated mechanisms rather than classical receptor-mediated pathways, consistent with effects reported for structurally related alkanes that disrupt membrane integrity and cellular viability. Pathway-level similarities between the current findings and our previous study on PFAS-exposed hepatocytes (Alijagic et al., 2024) were seen particularly at the lowest exposure concentration, where both exposures affected fatty acid activation, *de novo* fatty acid biosynthesis, PIP metabolism, glycosphingolipid metabolism, pyrimidine metabolism, and O-glycan biosynthesis. In contrast, fewer overlaps were evident at the highest F6H8 concentration, with only β-alanine metabolism, butanoate metabolism, and urea/amino group metabolism being commonly affected.

Several limitations should be acknowledged. Exposure levels were estimated based on data from structurally related compounds due to the absence of pharmacokinetic data on F6H8 absorption, distribution, and tissue accumulation. A previous study in rabbits (Kroesser et al., 2018) detected F6H8 in blood at high parts-per-billion (ppb) concentrations and indicated that repeated administration could lead to systemic enrichment. Given the lipophilic nature of F6H8 and evidence from similar compounds, hepatic accumulation is plausible.While the 24-hour exposure duration does not model chronic exposure per se, it represents a validated approach in hepatocyte metabolomics to capture stable metabolic reprogramming while minimizing secondary cytotoxic effects.. Furthermore, because F6H8 is administered ocularly in clinical use, our hepatocyte model does not replicate the initial site of exposure, and the findings should therefore be interpreted as reflecting potential systemic rather than local ocular effects. Nevertheless, this model has

been validated in prior studies investigating PFAS mixtures, producing metabolic patterns consistent with both *in vivo* animal data and human exposure profiles [36].

In conclusion, this study provides the first comprehensive evaluation of the metabolic effects of perfluorohexyloctane (F6H8) in human hepatocytes. Our findings indicate that F6H8 is not metabolically inert, may undergo biotransformation to PFAS-like carboxylic acids, and induces concentration-dependent metabolic reprogramming consistent with membrane perturbation, mitochondrial dysfunction, and oxidative stress. While derived from an in vitro system, these results raise important questions regarding the systemic safety of semifluorinated alkanes used in medical applications and underscore the need for longer-term *in vivo* studies addressing accumulation, metabolism, and chronic effects. Although these findings advance our understanding of cellular responses to F6H8, they derive from an in vitro system and should not be interpreted as direct evidence of adverse effects in humans.

CRediT authorship contribution statement

Andi Alijagic: Writing – review & editing, Methodology, Formal analysis, Conceptualization. **Jade Chaker:** Writing – review & editing, Methodology, Investigation. **João Marcos G. Barbosa:** Writing – review & editing, Investigation. **Daniel Duberg:** Writing – review & editing, Methodology, Investigation. **Victor Castro-Alves:** Writing – review & editing, Methodology, Investigation. **Alex M. Dickens:** Writing – review & editing, Methodology, Investigation. **Matej Orešič:** Writing – review & editing, Conceptualization. **Tuulia Hyötyläinen:** Writing – original draft, Visualization, Supervision, Methodology, Investigation, Formal analysis, Conceptualization.

Declaration of competing interest

The authors declare that they have no known competing financial interests or personal relationships that could have appeared to influence the work reported in this paper.

Acknowledgments

This study was supported by the Swedish Research Council (grants no. and 2020-03674 and 2016-05176 to T.H and M.O), Formas (grant no. to T.H and M.O), Novo Nordisk Foundation (Grants no. NNF20OC0063971 and NNF21OC0070309 to T.H. and M.O.), and by the “Investigation of endocrine-disrupting chemicals as contributors to progression of metabolic dysfunction-associated steatotic liver disease” (EDC-MASLD) consortium funded by the Horizon Europe Program of the European Union under Grant Agreement 101136259 (to MO and TH). The study was also partially supported by grant from the Swedish Knowledge Foundation (Grant 20220122).

We also thank Lorane Valgueblasse for help in the sample preparations. The authors would also like to thank the Turku Metabolomics Centre and Biocentre Finland for funding the instruments at the University of Turku used in this manuscript.

Views and opinions expressed are those of the author(s) only and do not necessarily reflect those of the European Union. Neither the European Union nor the granting authority can be held responsible for them.

Appendix A. Supplementary material

Supplementary data to this article can be found online at https://doi.org/10.1016/j.envint.2026.110112.

Data availability

We have shared a link with the data deposition site.

Metabolomics MS-based data are deposited in MassIVE repository (https://massive.ucsd.edu/) under the assigned code MSV000099594. The data is currently marked as private and can be accessed in reviewer mode with the following credentials:

Login: MSV000099594_reviewer

Password: ED_MetORU2025

References

Alijagic, A., Scherbak, N., Kotlyar, O., Karlsson, P., Wang, X., Odnevall, I., Benada, O., Amiryousefi, A., Andersson, L., Persson, A., Felth, J., 2023. A novel nanosafety approach using cell painting, metabolomics, and lipidomics captures the cellular and molecular phenotypes induced by the unintentionally formed metal-based (nano) particles. Cells 12 (2), 281. https://doi.org/10.3390/cells12020281.

Alijagic, A., Sinisalu, L., Duberg, D., Kotlyar, O., Scherbak, N., Engwall, M., Orešič, M., Hyötyläinen, T., 2024. Metabolic and phenotypic changes induced by PFAS exposure in two human hepatocyte cell models. Environ. Int. 190, 108820. https://doi.org/10.1016/j.envint.2024.108820.

Alijagic, A., Sinisalu, L., Duberg, D., Kotlyar, O., Scherbak, N., Engwall, M., Oresic, M., Hyotylainen, T., 2024. Metabolic and phenotypic changes induced by PFAS exposure in two human hepatocyte cell models. Environment International 190, 108820.

Apostolopoulou, M., Gordillo, R., Koliaki, C., Gancheva, S., Jelenik, T., De Filippo, E., Herder, C., Markgraf, D., Jankowiak, F., Esposito, I., et al., 2018. Specific hepatic sphingolipids relate to insulin resistance, oxidative stress, and inflammation in nonalcoholic steatohepatitis. Diabetes Care 41 (6), 1235–1243. https://doi.org/10.2337/dc17-1318 (acccessed 11/8/2023).

Balram, A., Thapa, S., Chatterjee, S., 2022. Glycosphingolipids in diabetes, oxidative stress, and cardiovascular disease: prevention in experimental animal models. Int J Mol Sci 23 (23), 15442. https://doi.org/10.3390/ijms232315442.

Cravedi, J.P., Tulliez, J., 1986. Metabolism of n-alkanes and their incorporation into lipids in the rainbow trout. Environ. Res. 39 (1), 180–187. https://doi.org/10.1016/s0013-9351(86)80020-2 From NLM.

Ferro, Y., Krafft, M.P., 2002. Incorporation of semi-fluorinated alkanes in the bilayer of small unilamellar vesicles of phosphatidylserine: impact on fusion kinetics. *Biochimica et Biophysica Acta (BBA) - Molecular and Cell Biology of*. Lipids 1581 (1), 11–20. https://doi.org/10.1016/S1388-1981(02)00116-6.

Gai, Z., Samodelov, S.L., Alecu, I., Hornemann, T., Grove, J.I., Aithal, G.P., Visentin, M., Kullak-Ublick, G.A., 2023. Plasma sphingoid base profiles of patients diagnosed with intrinsic or idiosyncratic drug-induced liver injury. Int J Mol Sci 24 (3), 3013. https://doi.org/10.3390/ijms24033013.

Geng, D., Musse, A.A., Wigh, V., Carlsson, C., Engwall, M., Orešič, M., Scherbak, N., Hyötyläinen, T., 2019. Effect of perfluorooctanesulfonic acid (PFOS) on the liver lipid metabolism of the developing chicken embryo. Ecotoxicol. Environ. Saf. 170, 691–698. https://doi.org/10.1016/j.ecoenv.2018.12.040.

Guillouzo, A., Corlu, A., Aninat, C., Glaise, D., Morel, F., Guguen-Guillouzo, C., 2007. The human hepatoma HepaRG cells: a highly differentiated model for studies of liver metabolism and toxicity of xenobiotics. Chem. Biol. Interact. 168 (1), 66–73. https://doi.org/10.1016/j.cbi.2006.12.003 From NLM.

Kariuki, M.N., Nagato, E.G., Lankadurai, B.P., Simpson, A.J., Simpson, M.J., 2017. Analysis of sub-lethal toxicity of perfluorooctane sulfonate (PFOS) to Daphnia magna using 1H nuclear magnetic resonance-based metabolomics. Metabolites 7 (2), 15.

Kim, S.-A., Lee, Y.-M., Choi, J.-Y., Jacobs, D.R., Lee, D.-H., 2018. Evolutionarily adapted hormesis-inducing stressors can be a practical solution to mitigate harmful effects of chronic exposure to low dose chemical mixtures. Environ. Pollut. 233, 725–734. https://doi.org/10.1016/j.envpol.2017.10.124.

Kroesser, S., Spencer, E., Grillenberger, R., Struble, C.B., Fischer, K., 2018. Ocular and systemic distribution of 14C-perfluorohexyloctane following topical ocular administration to rabbits. Investigative Ophthalmology & Visual Science 59 (9), 2656.

Krösser, S., Grillenberger, R., Eickhoff, K., Korward, J., Cavet, M.E., Mah, F.S., 2025. Ocular Pharmacokinetics and Biodistribution of Perfluorohexyloctane after Topical Administration to Rabbits. J. Ocul. Pharmacol. Ther. 41 (7), 370–377. https://doi.org/10.1089/jop.2025.0056.

Labine, L.M., Oliveira Pereira, E.A., Kleywegt;, S., Jobst, K.J., Simpson, A.J., Simpson, M. J., 2022. Comparison of sub-lethal metabolic perturbations of select legacy and novel perfluorinated alkyl substances (PFAS) in Daphnia magna. Environ. Res. 212, 113582. https://doi.org/10.1016/j.envres.2022.113582.

Li, S., Park, Y., Duraisingham, S., Strobel, F.H., Khan, N., Soltow, Q.A., Jones, D.P., Pulendran, B., 2013. Predicting network activity from high throughput metabolomics. PLoS Comput. Biol. 9 (7), e1003123. https://doi.org/10.1371/journal.pcbi.1003123 From NLM Medline.

Lu, Y., Pang, Z., Xia, J., 2022. Comprehensive investigation of pathway enrichment methods for functional interpretation of LC–MS global metabolomics data. Brief. Bioinform. 24 (1). https://doi.org/10.1093/bib/bbac553 acccessed 4/3/2024.

McCarthy, R.D., 1964. Mammalian metabolism of straight-chain saturated hydrocarbons. Biochimica et Biophysica Acta (BBA)-Specialized Section on Lipids and Related Subjects 84 (1), 74–79. https://doi.org/10.1016/0926-6542(64)90102-7.

Mertens, S., Bednarz, J., Engelmann, K., 2002. Evidence of toxic side effects of perfluorohexyloctane after vitreoretinal surgery as well as in previously established in vitro models with ocular cell types. Graefes Arch. Clin. Exp. Ophthalmol. 240 (12), 989–995. https://doi.org/10.1007/s00417-002-0561-0.

Napoli, M., Krotz, L., Conte, L., Seraglia, R., Traldi, P., 1993. Mass spectrometric studies on some $F(CF_2)n(CH_2)mH$ semifluorinated alkanes. Rapid Commun. Mass Spectrom. 7 (11), 1012–1016. https://doi.org/10.1002/rcm.1290071110.

Pang, Z., Lu, Y., Zhou, G., Hui, F., Xu, L., Viau, C., Spigelman, A.F., MacDonald, P.E., Wishart, D.S., Li, S., et al., 2024. MetaboAnalyst 6.0: towards a unified platform for

metabolomics data processing, analysis and interpretation. Nucleic Acids Res. 52 (W1), W398–W406. https://doi.org/10.1093/nar/gkae253.

Plassmann, M.M., Berger, U., 2010. Trace analytical methods for semifluorinated n-alkanes in snow, soil, and air. Anal. Chem. 82 (11), 4551–4557. https://doi.org/10.1021/ac1005519.

Rhea Lloyd, W. B., Wiley Chambers, Charles Ganley. Summary Review of NDA 216675. FDA: 2023.

Rose, S., Cuvellier, M., Ezan, F., Carteret, J., Bruyère, A., Legagneux, V., Nesslany, F., Baffet, G., Langouët, S., 2022. DMSO-free highly differentiated HepaRG spheroids for chronic toxicity, liver functions and genotoxicity studies. Arch. Toxicol. 96 (1), 243–258. https://doi.org/10.1007/s00204-021-03178-x From NLM.

Rossnerova, A., Izzotti, A., Pulliero, A., Bast, A., Rattan, S.I.S., Rossner, P., 2020. The molecular mechanisms of adaptive response related to environmental stress. Int. J. Mol. Sci. 21 (19), 7053.

Rotander, A., Ramos, M.J.G., Mueller, J.F., Toms, L.M., Hyötyläinen, T., 2024. Metabolic changes associated with PFAS exposure in firefighters: A pilot study. Sci Total Environ 953, 176004. https://doi.org/10.1016/j.scitotenv.2024.176004.

Sabín, J., Ruso, J.M., González-Pérez, A., Prieto, G., Sarmiento, F., 2006. Characterization of phospholipid+semifluorinated alkane vesicle system. Colloids Surf. B Biointerfaces 47 (1), 64–70. https://doi.org/10.1016/j.colsurfb.2005.11.022.

Schmid, R., Heuckeroth, S., Korf, A., Smirnov, A., Myers, O., Dyrlund, T.S., Bushuiev, R., Murray, K.J., Hoffmann, N., Lu, M., et al., 2023. Integrative analysis of multimodal mass spectrometry data in MZmine 3. Nat. Biotechnol. 41 (4), 447–449. https://doi.org/10.1038/s41587-023-01690-2.

Steven, P., Scherer, D., Krösser, S., Beckert, M., Cursiefen, C., Kaercher, T., 2015. Semifluorinated alkane eye drops for treatment of dry eye disease–a prospective, multicenter noninterventional study. J. Ocul. Pharmacol. Ther. 31 (8), 498–503. https://doi.org/10.1089/jop.2015.0048 From NLM.

Stolowich, N., Vittitow, J., Kissling, R., Borchman, D., 2023. Oxygen-carrying capacity of perfluorohexyloctane, a novel eye drop for dry eye disease. Curr. Ther. Res. Clin. Exp. 98, 100705. https://doi.org/10.1016/j.curtheres.2023.100705 From NLM PubMed-not-MEDLINE.

Sumner, L.W., Amberg, A., Barrett, D., Beale, M.H., Beger, R., Daykin, C.A., Fan, T.W., Fiehn, O., Goodacre, R., Griffin, J.L., et al., 2007. Proposed minimum reporting standards for chemical analysis chemical analysis working group (CAWG) metabolomics standards initiative (MSI). Metabolomics 3 (3), 211–221. https://doi.org/10.1007/s11306-007-0082-2 From NLM.

Tauber, J., Berdy, G.J., Wirta, D.L., Krösser, S., Vittitow, J.L., Alpern, L.M., Aune, C., Downing, J.E., El-Harazi, S., Evans, D.G., Goldberg, D., 2023. NOV03 for dry eye disease associated with meibomian gland dysfunction: results of the randomized phase 3 GOBI study. Ophthalmology 130 (5), 516–524. https://doi.org/10.1016/j.ophtha.2022.12.021.

Truong, L., Rericha, Y., Thunga, P., Marvel, S., Wallis, D., Simonich, M.T., Field, J.A., Cao, D., Reif, D.M., Tanguay, R.L., 2022. Systematic developmental toxicity assessment of a structurally diverse library of PFAS in zebrafish. J. Hazard. Mater. 431, 128615. https://doi.org/10.1016/j.jhazmat.2022.128615.

Tsagogiorgas, C., Theisinger, S., Heesch, E., Krebs, J., Holm, R., Beck, G., Yard, B., 2015. Evaluation of pharmacokinetic properties and anaesthetic effects of propofol in a new perfluorohexyloctane (F6H8) emulsion in rats – a comparative study. Int. J. Pharm. 486 (1), 69–76. https://doi.org/10.1016/j.ijpharm.2015.03.037.

Tulliez, J.E., Bories, G.F., 1978. Metabolism of an n-paraffin, heptadecane, in rats. Lipids 13 (2), 110–115. https://doi.org/10.1007/BF02533251.

Wang, K., Wang, R., Shan, W., Yang, Z., Chen, Y., Wang, L., Zhang, Y., 2024. Unravel the in-source fragmentation patterns of per- and polyfluoroalkyl substances during analysis by LC-ESI-HRMS. Environ. Sci. Technol. 58 (51), 22766–22776. https://doi.org/10.1021/acs.est.4c08442.

Zarif, L., Postel, M., Septe, B., Trevino, L., Riess, J.G., Mahé, A.-M., Follana, R., 1994. Biodistribution of mixed fluorocarbon–hydrocarbon dowel molecules used as stabilizers of fluorocarbon emulsions: a quantitative study by fluorine nuclear magnetic resonance (NMR). Pharm. Res. 11 (1), 122–127. https://doi.org/10.1023/A:1018914215345.

Zweigle, J., Bugsel, B., Zwiener, C., 2022. FindPFΔS: non-target screening for PFAS—comprehensive data mining for MS2 fragment mass differences. Anal. Chem. 94 (30), 10788–10796. https://doi.org/10.1021/acs.analchem.2c01521.